

Enhancing Modality-Agnostic Representations via Meta-Learning for Brain Tumor Segmentation

Aishik Konwer¹, Xiaoling Hu¹, Xuan Xu¹, Joseph Bae², Chao Chen², Prateek Prasanna²

¹Department of Computer Science, Stony Brook University

²Department of Biomedical Informatics, Stony Brook University

{akonwer, xiaolhu, xuaxu}@cs.stonybrook.edu

{joseph.bae, Chao.Chen.1, Prateek.Prasanna}@stonybrook.edu

Abstract

In the medical vision domain, different imaging modalities provide complementary information. However, in practice, not all modalities may be available during inference. Previous approaches, e.g., knowledge distillation or image synthesis, often assume the availability of full modalities for all patients during training; this is unrealistic and impractical owing to the variability in data collection across sites. We propose a novel approach to learn enhanced modality-agnostic representations by employing a novel meta-learning strategy in training, even when only a fraction of full modality patients are available. Meta-learning enhances partial modality representations to full modality representations by meta-training on partial modality data and meta-testing on limited full modality samples. Additionally, we co-supervise this feature enrichment by introducing an auxiliary adversarial learning branch. More specifically, a missing modality detector is used as a discriminator to mimic the full modality setting. Our segmentation framework significantly outperforms state-of-the-art brain tumor segmentation techniques in missing modality scenarios, as demonstrated on two brain tumor MRI datasets.

1. Introduction

In medical imaging, often multiple imaging modalities/protocols are acquired. Each modality provides complementary diagnostic and prognostic cues to clinicians. For instance, multiple 3D Magnetic resonance (MR) modalities, namely native T1, post-contrast T1-weighted (T1c), T2-weighted (T2), and Fluid Attenuated Inversion Recovery (FLAIR) are used together to understand the underlying texture and spatial complexity of brain tumors and their surroundings [3, 5]. Deep learning approaches [10, 21, 36, 47, 50, 57] have found great success in multimodal brain tumor

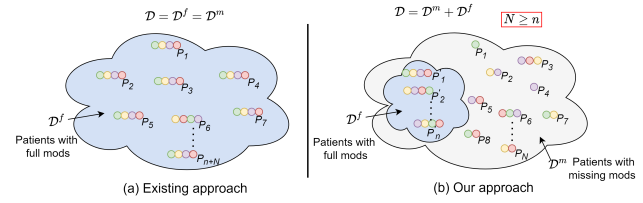


Figure 1. Comparison of the paradigms generally adopted by existing missing modality approaches (left) vs. our method (right) for brain tumor segmentation. N and n refers to number of patients with partial and full modalities respectively. Previous methods either utilize the full modality data \mathcal{D}^f for all patients or simulate missing scenarios to create partial modality data \mathcal{D}^m from the same. On the other hand, our approach works in a limited full modality setting $\mathcal{D}^f \leq \mathcal{D}^m$.

segmentation and treatment response assessment. These methods perform well only when all four acquisition modalities are available as input (i.e., in the full modality setting). However, in clinical practice, only a subset of modalities are often available due to image degradation, patient movement related artifacts [18], erroneous acquisition settings, brief scan times etc. Hence it is crucial to develop robust modality-agnostic methods which can achieve state-of-the-art performance in missing modality settings.

Over the past half decade, a plethora of works have been proposed to address missing modality scenarios during medical image segmentation. Two major categories of these works are: 1) Knowledge distillation: Such methods [2, 23, 42, 48, 51] propose to train individual student models for each missing modality scenario, and thereby learn privileged information from a full modality based teacher network. 2) Image synthesis: Several works [25, 41, 53, 54, 58] employ generative models to synthesize the missing modalities en route to segmentation. They utilize full modality images as ground truth while training a generative adversarial network (GAN) to reconstruct the missing modalities. It must be noted that these categories rely on the presence of

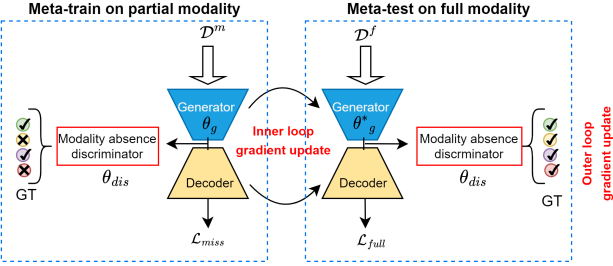


Figure 2. Overview of the proposed framework. \mathcal{D}^m and \mathcal{D}^f are used as inputs for encoder-decoder networks in meta-train and meta-test phase, respectively. Representations of partial modality data are adapted to full modality domain through 1) meta-optimization of gradients in both datasets, and 2) an adversarial learning based on predictions by a modality absence classifier.

full modality data for all patients in the training phase (see Fig. 1a). However, it is impractical to expect such an ideal case in real world datasets since missing instances can occur both during training and inference phases. Hence it is imperative to build models that can be trained under the assumption that only a fraction of patients contain full modality data (see Fig. 1b).

Another category of methods recently rising in popularity is shared latent space models [7, 8, 13, 14, 20, 22, 29, 31, 52, 55, 56, 59]; these methods learn a shared latent representation that is robust to missing modality scenarios. They fuse information from available modalities and exploit both intra- and inter-modal correlations to encode a common representation. Although most approaches in the third category do not depend on full modality data, they may suffer from the following drawbacks: 1) degraded quality of shared representations that do not incorporate the relevant and rich information generally existing in full modality data, 2) sub-optimal performance on subsets involving modalities which rarely occur during training (e.g. on T1+T1c+T2 if T1c is rare), as a consequence of learning biased mapping from available modalities. These observations motivate us to design a modality-agnostic network (see Fig. 2) that can jointly learn superior mapping and enriched shared representations even with limited complete data.

In this work we use meta-learning as a training strategy to achieve a unified framework that can tackle missing modalities in both training and inference. For this purpose, we divide the training dataset into two cohorts of patients having partial and full modality data, respectively. The former is used in meta-train phase to update the model parameters while the later is deployed during meta-testing. Our intention is to finetune the modality-agnostic representation learned from partial modality data. We also employ an adversarial learning technique which further enhances the quality of this shared representation. This is specifically achieved by using a multi-label classifier as discriminator. The discriminator predicts the presence/absence of

modalities in a fused latent representation by performing a binary classification for each modality. Our ultimate goal is to hallucinate the full modality representation from the hetero-modal feature space. Note that due to hetero-modal nature of the data, the number of available modalities can vary hugely across patients. To address this, we introduce a novel channel-attention weighted fusion module that can accept varying number of representations as input but generates a single fused output. Overall, our contributions can be summarized as follows:

- We propose a meta-learning paradigm to handle the hybrid nature of data (partial and full modalities) during training, and also enhance the shared representation (learned from partial modalities) to mimic a full modality representation. This adaptation is accomplished by meta-training on partial modality data while finetuning on full modality data during meta-test.
- We introduce a novel adversarial learning strategy that can further enrich the shared representations in the latent space. It overcomes the need of synthesizing missing modality images for a downstream task.
- We also present a modality-agnostic feature aggregator that weighs the available modalities via channel attention, to generate an unified encoded representation.

2. Related Work

Segmentation with missing modalities. Incomplete data is a long-standing issue in computer vision; it particularly has significant implications in medical vision. Data labeling is an expensive process which leads to a scarcity of high-fidelity annotations [26, 40, 49]. Due to privacy concerns and budget constraints, one or more modalities (audio/visual/text) [6, 11, 15, 28, 46] of the same data may not be available. In this work we focus on partial medical imaging modalities for brain tumor segmentation. Note that MRI ‘protocols’ or ‘sequences’ are referred to as ‘modalities’ here. Existing methods on complete multi-modal brain tumor segmentation [10, 21, 36, 47, 50, 57] perform poorly in realistic hetero-modal settings.

Researchers have broadly used three techniques to perform brain tumor segmentation from missing modalities including *knowledge distillation* (KD) [2, 23, 42, 48, 51], *generative modeling* [25, 41, 53, 54, 58] and *shared representation learning* [7, 8, 13, 14, 20, 22, 29, 31, 52, 55, 56, 59]. HAD-Net [48] pre-trains a teacher network with all modalities which transfers knowledge at multiple resolutions to a student model trained without T1c. ACN [51] trains a separate teacher-student pipeline for each subset of modalities. SMU-Net [2] exploits content and style matching modules for such distillation. Among the generative models, MM-GAN [41] uses a U-Net generator to impute missing modal-

ties while a PatchGAN learns to discriminate between real and synthesized inputs. MouseGAN [54] pre-trains a modality mapping component to synthesize all modalities from available ones. This module then generates missing modalities en route to segmentation. One major drawback of KD and GAN-based approaches is their inability to perform when not all modalities are present for a patient during training. Also, both techniques are time consuming and computationally expensive. Moreover, the unstable and non-converging nature of a 3D generator may lead to degraded quality of synthesized images, eventually affecting downstream performance.

Our method belongs to the third category of common latent space models. In [14, 22], the authors compute variational statistics (mean, variance) to construct unified representations for segmentation. Chartsias et. al [7] obtain fused representations by minimizing inter-modal feature distances. Multi-source information is modeled using correlation constraint [59] or region-aware fusion blocks [13] to encode shared representations. Recent frameworks [55, 56] in this genre advocate for exploiting intra/inter-modality relations through graph and transformer-based modeling. Such approaches usually lack flexibility for adaptation to all missing scenarios. They yield sub-optimal performance due to failure in retrieval of discriminative features generally existing in full modality data. Furthermore, these approaches can learn biased mappings among the available modalities leading to poor generalizable performance for modalities not encountered in training.

Meta-learning. Meta-learning algorithms [16, 37, 45] are inspired by human perception of new tasks. They utilize prior information learnt across similar events. Recently, optimization-based meta-learning [1, 16, 37] has gained popularity since they can easily encode prior information through an optimization process. Model-agnostic meta-learning (MAML) [43] is the most commonly used algorithm under this category, owing to its flexible application to any network trained through gradient descent. Researchers have widely adopted MAML frameworks to generalize a model to new tasks, unseen domains, and enriching input features in multimodal scenarios [30, 33]. SMIL [32] introduces a Bayesian MAML framework which attains comparable classification performance across both partial and full modality data. However their approach requires prior reconstruction of the missing modalities. HetMAML [9] proposes a modality-agnostic architecture that can handle heterogeneous task distributions, i.e. different modality combinations for input space. However, HetMAML does not attempt to attain generalizable performance across partial and full modalities. Inspired by the above two approaches, we propose a modified version of MAML that can not only accept hetero-modal inputs, but also enhance their representations with the additional information present in full set of

modalities. This leads to better segmentation performance for any hetero-modal input instance.

Domain adaptation. Domain adaptation refers to the training of a neural network to jointly generate both discriminative and domain-invariant features in order to model different source and target data distributions. Many approaches resort to distribution matching through source re-weighting [17], geometric transformation [4] or application of MMD and CORAL losses [19, 27, 44]. Rather than adapting distributions, we are more interested in adapting the partial modality (source domain) feature representations to the full modality (target domain) representations. Authors in [17] leverage an auxiliary domain classifier to address the domain shift. Inspired by their approaches, we design our discriminator as a modality absence predictor. Similar to Sharma et. al [41], we feed our discriminator with the correct modality code as ground truth, while the generator is provided an ‘all-one’ full modality code impersonating the presence of all modalities. In an attempt to fool the discriminator, the generator pushes itself to always mimic full modality representations, irrespective of the available inputs. This results in enhanced representations that boost downstream performance in missing modality situations.

3. Methodology

Overview. Given heterogeneous modalities as input, our goal is to build a modality-agnostic framework that can be robust to missing modality scenarios, and achieve performances comparable to a full modality setting. We have limited access to full modality data during training; this simulates a practical clinical scenario where brain tumor segmentation may need to be performed with partial modalities. To address this data-scarce situation, we aim to establish a mapping between partial and full modality representations. Our proposed approach is shown in Fig. 3. Meta-learning has been shown to be an efficient computational paradigm in dealing with heterogeneous training data [9], or conducting feature adaptation between different domains [32]. To this end, we adapt model-agnostic meta-learning to leverage information from both partial and full modality data. This strategy is elaborated in Sec. 3.1. We also want to further enrich encoded representations obtained from available modalities, with the supplemental information contained in full modality representations. More specifically, we propose a novel adversarial learning technique introducing a discriminator that acts as a modality absence classifier. A detailed description is provided in Sec. 3.3. Because we need to generate a common fused representation for each hetero-modal input combination, our architecture incorporates a novel feature aggregation module (see Sec. 3.2).

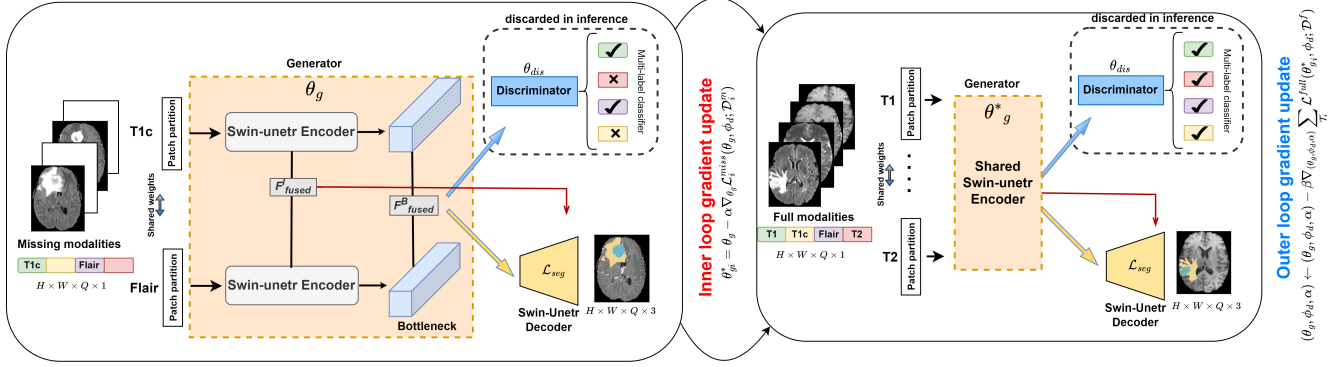


Figure 3. Illustration of the proposed framework. Available or full set of modalities are passed through a shared generator in meta-train and meta-test stages respectively. The aggregation module helps to obtain a fused representation from five different levels (level l and bottleneck are indicated here). Next, only the bottleneck embedding is used by the discriminator to predict which modalities are present at input. All the five fused embeddings are used by the segmentation decoder. Inner and outer loop gradient updates refer to the losses calculated in the meta-train and meta-test stages on partial modality and full modality data, respectively.

Algorithm 1 Modality-Agnostic Meta-Learning

```

1: Input: Training dataset  $\mathcal{D}$  is divided into two cohorts of patients with partial/missing and full modalities respectively  $\mathcal{D}^{tr} = \{\mathcal{D}^m, \mathcal{D}^f\}$ ;  $\beta$  as learning rate.
2: Initialise: Initialise  $\theta_g, \phi_d = \{\theta_{dis}, \theta_{dec}\}, \alpha$ 
3: Output: Optimized meta-parameters  $\{\theta_g, \phi_d, \alpha\}$ 
4: while not converged do
5:   Sample a batch of tasks  $\mathcal{T}^i \sim \{P(\mathcal{T})\}$ 
6:   for each task  $\mathcal{T}^i$  do
7:     Evaluate inner loop loss:  $\mathcal{L}_i^{miss}(\theta_g, \phi_d; \mathcal{D}_i^m)$ 
8:     Adapt:  $\theta_{gi}^* = \theta_g - \alpha \nabla_{\theta_g} \mathcal{L}_i^{miss}(\theta_g, \phi_d; \mathcal{D}_i^m)$ 
9:     Compute outer loop loss:  $\mathcal{L}^{full}(\theta_{gi}^*, \phi_d; \mathcal{D}^f)$ 
10:   end for
11:   Update meta-parameters:  $(\theta_g, \phi_d, \alpha) \leftarrow (\theta_g, \phi_d, \alpha) - \beta \nabla_{(\theta_g, \phi_d, \alpha)} \sum_{\mathcal{T}_i} \mathcal{L}^{full}(\theta_{gi}^*, \phi_d; \mathcal{D}^f)$ 
12: end while

```

3.1. Meta-Learning for Feature Adaptation

Suppose we have total M MR imaging modalities for a patient in the input space. Now, to simulate a real world scenario where full modalities are only available for a fraction of patients, some MRIs are randomly dropped for each patient during training. This training paradigm ensures the model to become more robust to missing scenarios at inference. Thus we construct a heterogeneous task distribution $P(\mathcal{T})$ that is a collection of k task distributions: $P(\mathcal{T}^1), P(\mathcal{T}^2), \dots, P(\mathcal{T}^k)$. Each such distribution $P(\mathcal{T}^i)$ has a distinct input feature space related to a specific subset of modalities. We however exclude the full modality subset from the task distribution due to its utilization in meta-testing, as explained in the following paragraph. Overall k types of task instances can be sampled from $P(\mathcal{T})$, where $k = 2^M - 2$.

Formally, we have a hetero-modal training dataset \mathcal{D} which we divide into two cohorts of patients $\{\mathcal{D}^m, \mathcal{D}^f\}$

containing partial and full modalities, respectively. The goal is to effectively learn from both types of data. We construct a batch of patients \mathcal{D}_i^m corresponding to each $P(\mathcal{T}^i)$.

Shared encoders are used along with a fusion module to produce a modality-agnostic representation. In our case, both encoder and fusion modules jointly constitute the generator which is represented as E_{θ_g} (parameterized by θ_g). An MLP-based classifier network, parameterized by θ_{dis} , is employed as discriminator as explained in Sec. 3.3. For clarity, parameters of the discriminator and decoder network, $\{\theta_{dis}, \theta_{dec}\}$, are collectively symbolized as ϕ_d . Our aim is to obtain an optimal generator parameter θ_g through task-wise training on \mathcal{D}_i^m by reducing the inner loop objective \mathcal{L}_i^{miss} .

$$\theta_{gi}^* = \theta_g - \alpha \nabla_{\theta_g} \mathcal{L}_i^{miss}(\theta_g, \phi_d; \mathcal{D}_i^m), \quad (1)$$

where α is a learnable rate for inner-level optimization. The optimized model is expected to perform better on \mathcal{D}^f . The goal of the updated framework is to accomplish the outer loop objective \mathcal{L}^{full} across all sampled tasks:

$$\min_{\theta_g, \phi_d} \sum_{\mathcal{T}_i} \mathcal{L}^{full}(\theta_{gi}^*, \phi_d; \mathcal{D}^f). \quad (2)$$

Both the inner and outer loop losses are kept as the same, referring to the generator and discriminator losses, \mathcal{L}_E and \mathcal{L}_{dis} . By forcing the partial modality trained model to perform well on full modality data, we implicitly target to recover the relevant information for better segmentation in missing modality scenarios. This partial to full modality mapping in feature space, is further strengthened by the introduction of a domain-adaptation inspired feature enrichment module. Further details can be found in Sec. 3.3. All three model meta parameters $(\theta_g, \phi_d, \alpha)$ are henceforth meta-updated by averaging gradients of outer loop loss over

a meta-batch of tasks.

$$(\theta_g, \phi_d, \alpha) \leftarrow (\theta_g, \phi_d, \alpha) - \beta \nabla_{(\theta_g, \phi_d, \alpha)} \sum_{\mathcal{T}_i} \mathcal{L}^{full}(\theta_g^*, \phi_d; \mathcal{D}^f). \quad (3)$$

Thus during meta-training, the model tunes its initialization parameter to achieve improved generalizability across all missing modality tasks. And then in the meta-test phase, by finetuning with full modality data, we map the learned feature representations to full modality space. Different from MAML, the pretrained model is directly evaluated on datasets where patients contain a fixed subset of modalities (one of the tasks \mathcal{T}^i already encountered in meta-training) at the inference stage. The training process is summarized in Algorithm 1.

3.2. Modality-Agnostic Feature Aggregation

We aim to utilize multiple modalities (which vary in number per patient) and derive a common fused representation. Individual encoders E_1, E_2, \dots, E_n having shared parameters are trained to extract features from each of the n available patient-specific modalities, where $1 \leq n \leq M$. These features $\mathbf{F}_1^l, \mathbf{F}_2^l, \dots, \mathbf{F}_n^l$ obtained from the corresponding levels (l) of each encoder are passed into a feature aggregation module. The aggregated representation, \mathbf{F}_{fused}^l (depicted in Fig. 4), is eventually used as input to the decoder for segmentation.

For a particular level l , a modality feature $\mathbf{F}_j^l \in \mathbb{R}^{C \times H \times W \times Q}$ includes C channels and feature maps of size $H \times W \times Q$ where $j \in \{1, 2, \dots, n\}$. The channels in these generated features are considered to encode relevant tumor-class specific information. Our fusion block exploits the correlation among available modality representations to come up with a unified feature that best describes the tumor characteristics of a particular patient. First, the channel information γ_j^l of a modality at level l is preserved through the following equation:

$$\gamma_j^l = gap(\mathbf{F}_j^l) = \frac{1}{H \times W \times Q} \sum_{h=1}^H \sum_{w=1}^W \sum_{q=1}^Q \mathbf{F}_j^l(h, w, q), \quad (4)$$

where $j \in \{1, 2, \dots, n\}$ and gap denotes Global Average Pooling operation. Following this, we not only concatenate $\gamma_1^l, \gamma_2^l, \dots, \gamma_n^l$, but also impute zeros in the channel information of $(M - n)$ missing modalities to form a resultant M -dimensional vector γ^l .

$$\gamma^l = \gamma_1^l \oplus \gamma_2^l \oplus \gamma_3^l \dots \oplus \gamma_M^l, \quad (5)$$

γ^l is mapped to the channel weights of M modality features through a multi-layer perceptron (MLP) and sigmoid activation function, σ .

$$\Gamma^l = \sigma(MLP(\gamma^l)). \quad (6)$$

Though Γ^l contains M scalar values, only the weights of n available modalities are multiplied with their corresponding features. These weighted features are finally summed to obtain the fused representation \mathbf{F}_{fused}^l .

$$\mathbf{F}_{fused}^l = \sum_{j=1}^n \Gamma_j^l \mathbf{F}_j^l. \quad (7)$$

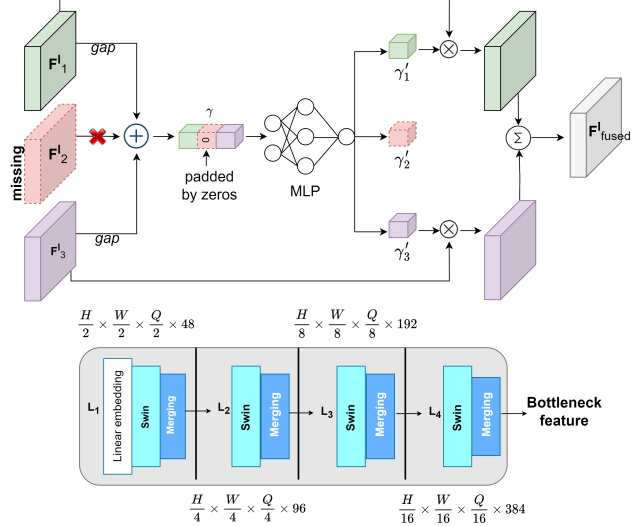


Figure 4. Illustration of the proposed feature aggregation module. Modality \mathbf{F}_2^l is missing. The two available modalities, \mathbf{F}_1^l and \mathbf{F}_3^l are passed through global average pooling (gap) operation and eventually fed into an MLP to generate the shared representation \mathbf{F}_{fused}^l . A schematic of the adopted Swin-UNETR encoder is also provided.

3.3. Adversarial Feature Enrichment

Considering that the full modality contains richer information, we enforce the encoder outputs to mimic their representations, irrespective of the input combination. The modality encoders and fusion module can be collectively considered as a shared generator E . We then introduce a MLP based multi-label classifier as our discriminator D .

The objective of D is to predict the absence/presence of modalities from the fused embedding \mathbf{F}_{fused}^B at the bottleneck level. D utilizes Binary Cross-Entropy loss \mathcal{L}_{BCE} , and sigmoid activation to output M binary predictions \hat{d} , denoting whether a modality is available or not. While calculating the discriminator loss \mathcal{L}_{dis} indicated below, the ground truth variable T_{real} is a vector of size M which reflects the true combination of modalities available at input for that iteration. For example, assuming that $M = 4$, and only first two modalities are available, $T_{real} = \{1, 1, 0, 0\}$.

$$\mathcal{L}_{dis} = \sum_{z=1}^{\mathcal{D}^m + \mathcal{D}^f} \mathcal{L}_{BCE}(\hat{d}_z, T_{real_z}). \quad (8)$$

The generator loss is a combination of segmentation loss and an adversarial loss used to train the generator to fool the discriminator. We consider a dummy ground truth variable T_{dummy} . In order to encourage the generator to encode representations that confuse or “fool” the discriminator into inferring that all modalities are present, we set $T_{dummy} = \{1, 1, 1, 1\}$, masquerading all generated representations as full modality representations. Thus D pushes the generator G to agnostically produce full modality representations.

$$\mathcal{L}_E = \lambda_1 \mathcal{L}_{Seg} + \lambda_2 \sum_{z=1}^{\mathcal{D}^m + \mathcal{D}^f} \mathcal{L}_{BCE}(\hat{d}_z, T_{dummy_z}). \quad (9)$$

We adopt Swin-UNETR [47] architecture that employs soft Dice loss [35] to perform voxel-wise semantic segmentation. The segmentation loss function \mathcal{L}_{seg} is defined as follows:

$$\mathcal{L}_{seg}(G, P) = 1 - \frac{2}{V} \sum_{v=1}^V \frac{\sum_{u=1}^U G_{u,v} P_{u,v}}{\sum_{u=1}^U G_{u,v}^2 + \sum_{u=1}^U P_{u,v}^2}.$$

where V is the number of classes and U is the number of voxels. $P_{u,v}$ and $G_{u,v}$ refer to the predicted output and one-hot encoded ground truth for class v at voxel u , respectively.

4. Experiment Design and Results

To validate our framework against various missing scenarios, we evaluate brain tumor segmentation results on all fifteen combinations of the four image modalities for a fixed test set. The average score is also reported for comparisons.

Datasets. We use two segmentation datasets from BRATS2018 and BRATS2020 challenge [34]. They comprise 285 and 369 training cases respectively. All patients have $M = 4$ sequences of MR scans. To utilize 3D information we perform volumetric segmentation with the $155 \times 240 \times 240$ images. As part of pre-processing, the organizers skull-stripped the volumes and interpolated them to an isotropic 1mm^3 resolution. For a given patient, the four sequences have been co-registered to the same anatomical template. The segmentation classes include whole tumor (WT), tumor core (TC), and enhancing tumor (ET).

Implementation details. The architecture is implemented in Pytorch 1.7 [39] and experiments are performed on a server with three 48 GB Nvidia Quadro RTX 8000 GPUs. We randomly drop modalities during training to construct the missing-modality dataset \mathcal{D}^m . We ablate the fraction of patients reserved for full modality dataset \mathcal{D}^f (Fig. 6a). Our method adopts a modified Swin-UNETR [47] housing up to 4 encoders E_1, E_2, E_3, E_4 which are Swin transformers. The images are first resized to $128 \times 128 \times 128$. Features are extracted from 5 different levels of each encoder. We randomly split the BRATS2018 dataset into 200 and 85 patients for training and testing, and the BRATS2020 dataset

into 269 and 100 for training and testing, respectively. Augmentations including random rotations, intensity shifts, and mirror flipping, are applied to the resized images. The foreground voxels within brain are intensity-normalized to zero mean and unit standard deviation. We train our network using AdamW optimizer with an outer loop learning rate $\beta = 5e-4$ for a maximum of 500 epochs. The batch size per task is kept as 1. During meta-training, we consider a metabatch size of 8, i.e., our meta-batch comprises 8 different modality-combinations, each representing a separate task \mathcal{T}_i . The two hyperparameters λ_1 and λ_2 in generator loss \mathcal{L}_E are taken as 0.8 and 0.2, respectively. During training, \mathcal{L}_{dis} is multiplied by 0.5 to prevent it from overpowering the generator. More details can be found in the supplementary (Sec. 15). During inference, the meta-pretrained model is evaluated on test sets where all patients have a fixed subset of modalities. The discriminator is discarded at the inference stage.

Performance metrics. Dice similarity coefficient (DSC \uparrow) is used (Tab. 1) to evaluate segmentation performance.

4.1. Comparisons with State-of-the-art

Quantitative results: In Tab. 1, we compare our approach with SOTA methods including HeMIS [22], U-HVED [14], D2-Net [52], ACN [51], RFNet [13] and mmFormer [55] for tumor segmentation on BRATS2018 dataset. HeMIS, U-HVED and D2-Net learn a biased mapping among available modalities by simulating missing scenarios and project it into a shared representation. Hence their overall performance is lower compared to ACN which co-trains with the full modality of all samples. Recent shared latent space models like mmFormer and RFNet perform comparably to ACN. They either focus on learning inter-modal correlations or tumor region-aware fused representations. Our method utilizes full modality from only 50% samples, and yet outperforms these approaches. We thus excel in efficient utilization of full modality data. In comparison with the second-best approach in WT, TC and ET, our average DSC shows improvements of 0.89% (over mmFormer), 1.96% (over ACN) and 1.68% (over ACN), respectively. Although ACN pursues a KD-driven approach to achieve the partial-to-full modality mapping, it ends up building a combinatorial number of models dedicated to each subset. This leads to a highly cost-ineffective solution which is also based on the impractical scenario that all samples contain full modality data. In our framework, we mimic this distillation learning even in a shared latent model through efficient application of meta-learning and adversarial training. It can be seen from Tab. 1 that our method surpasses all other approaches in 39 out of 45 multi-modal combinations across the tumor regions. The standard deviation and p-values on BRATS2018 are reported in Sec. 12 of supplementary. We also evaluated all methods via Hausdorff Distance (HD95)

M	FLAIR	○	○	○	●	○	○	●	○	●	●	●	●	○	●	●	Avg
	T1	○	○	●	○	○	●	●	○	○	●	●	●	○	●	●	
	T1c	○	●	○	○	●	●	○	○	●	●	●	●	○	●	●	
	T2	●	○	○	○	●	●	○	●	●	●	●	●	●	●	●	
WT	HeMIS [22]	79.85	60.32	55.76	66.20	81.63	65.39	75.41	81.70	82.56	76.25	79.82	84.58	86.27	82.74	85.06	76.23
	U-HVED [14]	81.06	58.74	52.37	82.65	80.88	66.21	83.70	82.83	86.44	84.92	86.33	87.56	87.84	83.47	88.25	79.55
	D2-Net [52]	76.58	43.79	19.43	85.06	84.62	65.37	86.18	82.56	86.35	87.94	87.31	88.59	89.12	83.78	88.94	77.04
	ACN [51]	85.24	79.16	78.65	86.72	85.87	79.27	86.33	85.21	86.69	87.54	86.92	88.22	87.51	86.38	89.14	85.25
	RFNet [13]	84.92	73.41	72.57	87.93	86.22	78.31	89.43	86.81	89.98	89.23	89.80	90.22	90.16	86.95	90.32	85.75
	mmFormer [55]	84.73	76.10	75.39	88.53	86.75	79.24	89.57	86.61	90.05	89.69	89.64	90.11	90.20	87.11	90.09	86.25
	Ours	86.52	79.23	78.66	87.45	86.77	79.60	89.94	86.71	90.82	90.13	90.38	90.74	90.63	88.09	91.26	87.12
TC	HeMIS [22]	49.63	53.75	24.80	32.91	70.28	64.29	45.62	54.36	54.93	69.40	72.57	62.38	75.51	73.94	74.18	58.57
	U-HVED [14]	56.62	64.50	36.77	54.38	74.46	65.29	59.03	58.66	62.57	73.14	75.85	63.72	73.52	76.81	72.96	64.55
	D2-Net [52]	59.87	64.29	20.32	50.84	81.06	77.96	62.54	64.18	61.70	82.45	79.38	67.52	81.47	80.23	80.94	67.65
	ACN [51]	67.24	84.35	70.49	67.38	84.70	83.92	70.61	73.58	70.66	82.17	84.35	67.08	81.94	84.32	84.73	77.16
	RFNet [13]	67.72	78.87	64.39	67.85	83.04	80.84	72.80	71.65	73.32	83.76	84.09	74.89	84.26	82.98	84.40	76.99
	mmFormer [55]	65.92	77.50	62.94	66.10	80.58	79.35	72.31	69.89	71.39	79.72	81.53	73.30	80.68	80.56	81.62	74.89
	Ours	68.12	84.57	71.24	68.75	85.67	84.39	73.48	72.90	73.71	84.97	85.43	75.62	84.75	86.56	86.77	79.12
ET	HeMIS [22]	22.47	56.20	7.89	9.64	64.07	65.66	17.73	26.95	27.42	65.83	70.35	30.18	68.97	69.52	73.80	45.11
	U-HVED [14]	27.82	61.24	11.06	22.35	68.93	65.79	24.57	24.46	35.80	69.31	71.42	32.14	70.66	69.98	71.20	48.44
	D2-Net [52]	22.83	69.52	15.34	12.96	70.45	71.38	14.06	19.32	17.79	69.25	68.31	23.66	67.14	68.56	67.72	45.22
	ACN [51]	43.26	78.57	40.89	42.14	74.95	75.88	42.73	47.80	44.39	76.72	76.33	41.61	75.54	75.27	76.79	60.85
	RFNet [13]	40.62	69.73	37.62	38.08	75.42	71.55	45.67	43.44	45.36	75.18	76.52	47.14	76.75	75.26	76.71	59.67
	mmFormer [55]	39.65	66.23	37.08	38.72	68.70	67.84	45.15	42.61	43.69	68.42	68.36	45.33	68.45	69.81	68.16	55.88
	Ours	44.87	78.09	41.12	43.94	77.16	77.58	45.81	46.25	48.63	77.29	76.04	48.22	77.92	76.71	78.30	62.53

Table 1. Comparison with state-of-the-art (DSC %) for the different combinations of available modalities on BRATS2018. Dice scores are computed for three nested tumor subregions - Whole tumor (WT), Tumor core (TC), Enhancing tumor (ET). The best and second best scores are **highlighted** and underlined. Modalities present are denoted by ●, the missing ones by ○.

scores on BRATS2018. They can be found in Tab. 10 of supplementary. We also compare our approach with three SOTA methods on BRATS2020 in Tab. 2. For BRATS2020, the average DSC of the three tumor areas are boosted by 1.78%, 2.84% and 3.13%, respectively. A complete table with all combinations has been provided in supplementary.

Qualitative results: In Fig. 5 we visualize the segmentation masks predicted by U-HVED, RFNet and ours from four combinations of modalities. Unlike theirs, our segmentations do not degrade sharply as additional modalities are dropped during inference phase. Even with single T2 or T1c+T2 modalities, we achieve decent segmentation maps.

4.2. Ablation Studies

Effectiveness of adversarial and meta-learning. We perform several ablations to evaluate and justify the contribution of each proposed module in our architecture. First, we remove both the Adversarial and the Meta-training strategies to perform segmentation from only fusion of available modalities. We thus formulate a baseline, *mDrop*, where we include our feature-aggregation block to generate a fused representation from available modalities. *mDrop* solely learns the intra-model relations through transformer-based encoders and inter-modal dependencies through channel-weighted fusion. Tab. 3 shows that the average DSC of our model outperforms *mDrop* by 5.45%, 6.71% and 10.47% in the three tumor regions. Hence it is evident that solely

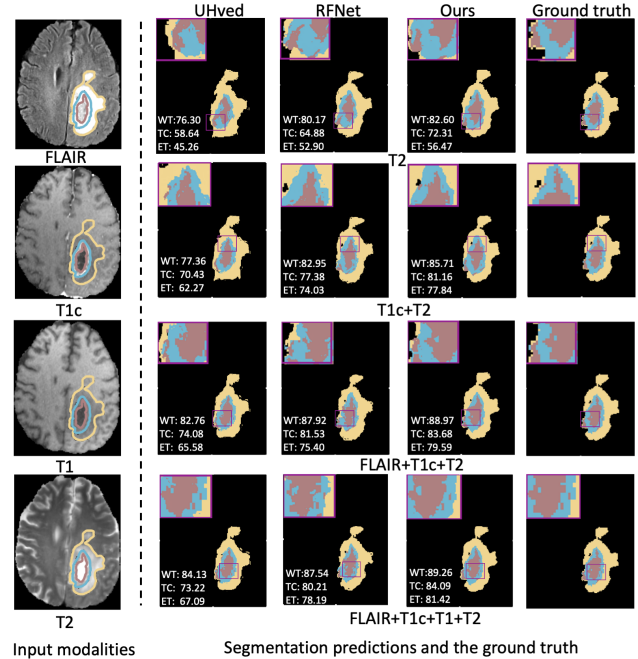


Figure 5. Qualitative comparisons with state-of-the-art methods. Column 1: four MRI modalities. Column 2-4: segmentation maps predicted by three methods for different combinations of modalities. Column 5: Ground truth. Our method is able to better capture gaps/islands (rows 1,3) and boundaries (row 4) in TC segmentations.

Methods	Average DSC (%)		
	WT	TC	ET
HeMIS [22]	77.29	67.12	49.64
U-HVED [14]	82.65	69.08	51.53
RFNet [13]	86.96	78.79	62.14
Ours	88.74	81.63	65.27

Table 2. Comparison on BRATS2020.

Methods	Average DSC (%)		
	WT	TC	ET
mDrop	81.67	72.41	52.06
+ GAN	84.49	75.38	55.64
+ MetaL	85.96	77.23	59.85
+ GAN + MetaL	87.12	79.12	62.53

Table 3. Ablation for major components.

Methods	Average DSC (%)		
	WT	TC	ET
Sum	85.99	78.21	60.85
Average	86.14	78.36	61.30
Att-pool	86.93	79.07	62.28
Ours	87.12	79.12	62.53

Table 4. Ablation study on fusion.

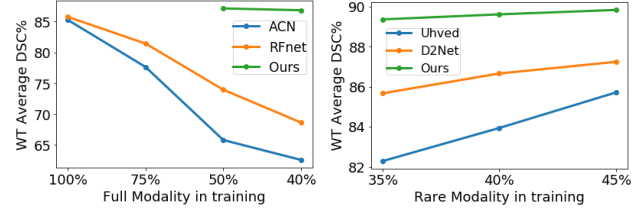
the modality-agnostic representations obtained from fusion of available modalities cannot generate accurate segmentations. This necessitates a feature enrichment technique that can improve the quality of the fused representation. We develop two variants through gradual introduction of our discriminator and meta-learning strategy as enrichment techniques. The enhanced representations are evaluated both quantitatively and qualitatively in supplementary (Sec. 14). As seen in Tab. 3, both variants surpass mDrop considerably. Meta-learning (MetaL) proved to be slightly better since we explicitly divide the dataset into missing and full modality samples for performing meta-training and meta-testing, respectively. Finally we arrive at an end-to-end meta-learning framework that also benefits from auxiliary supervision provided by the adversarial discriminator.

Ablation on aggregation block. We design 3 baseline aggregation modules to highlight the contribution of our proposed fusion strategy. These include: 1) channel-wise summation (Sum), 2) channel-wise averaging (Average), and 3) passing the accessible modalities individually through GAP and a global FCN for attention based pooling (Att-pool). Architectural details in supplementary. Tab. 4 indicates that our channel-attention based fusion provides a more sophisticated solution via concurrent handling of varying input modalities and inducing channel interaction among them.

Robustness to full modality setting. Due to the meta-learning strategy incorporated while training on hybrid data, we hypothesize that our network is robust to the ratio of full modality samples used in training. We compare against ACN and RFNet by varying the full modality count from 100% to 40% (Fig. 6a). In order to retain sufficient samples for each combination task in meta-training, we assume that at least 50% of the patients have partial modalities. Hence we show our results only on 50% and 40% proportions of full modality data. The fact that even with 50% full modality samples, we can match the evaluation scores of SOTA at 100% setting, is noteworthy. A sharp degradation can be noticed in the average WT DSC of SOTA once the number of full modality data decreases. On the other hand, our method shows only a minor drop of 0.29%. This is due to ACN being heavily dependent on full modality for knowledge distillation. RFNet, on the other hand, may not utilize full modality but suffers from an architectural drawback that requires full modality to be used as input. It under-fits since their overall sample count decreases. Our method ef-

ficiently utilizes even limited samples of full modality for feature adaptation in meta-testing. More importantly, the proposed architecture allows for variable number of input modalities thanks to the feature aggregation module. Owing to the above reasons, our approach is resilient to change in full modality proportion. Results for other tumor regions (TC, ET) are provided in supplementary.

Bias to presence of a specific modality. We also hypothesize that our model is robust to the scenario when a modality appears rarely during training. Tab. 5 demonstrates that when only 35% of FLAIR is considered for training, our method consistently outperforms U-HVED and D2-Net in all the 8 inference scenarios involving FLAIR. Our average DSC (89.37, 78.11 and 60.80) for WT, TC and ET are significantly higher than the second-best method (85.68, 68.77 and 47.07). We attribute this improvement to meta-learning which precludes the model from learning a biased mapping among available modalities by aligning the shared representations to full modality representations. Further experiments in Fig. 6b demonstrate that performance of U-HVED and D2-Net are highly sensitive to availability of a particular modality while our approach is impervious to this. On increasing FLAIR from 35% to 45%, our WT gain (+0.47%) is much lower than U-HVED (+3.42%) or D2-Net (+1.57%). Detailed results are provided in supplementary.



(a) Ablation results for varying % of full modality in training. (b) Ablation results for varying % of FLAIR in training.

Figure 6. Ablation studies.

Robustness to backbone variants. The proposed meta and adversarial training strategies are robust to any employed backbone including 3DUnet [12], nnUnet [24] and AttentionUnet [38]. Comparisons are provided in supplementary.

5. Conclusion

This paper presents a novel training strategy to address the problem of missing modalities in brain tumor segmentation under limited full modality supervision. We

M	FLAIR	•	•	•	•	•	•	•	•	Avg
WT	T1	○	●	○	○	●	●	○	●	
	T1c	○	○	○	●	●	○	●	●	
	T2	○	○	●	○	○	●	●	●	
	U-HVED	76.61	78.94	83.98	80.47	82.76	84.39	85.08	86.25	82.30
TC	D2-Net	82.44	83.79	85.16	85.55	85.18	87.63	88.02	87.70	85.68
	Ours	86.53	88.77	90.05	89.41	89.49	90.13	90.07	90.55	89.37
	U-HVED	50.23	55.46	57.35	71.85	74.31	59.02	72.19	71.40	63.97
ET	D2-Net	47.19	59.98	59.65	81.23	77.44	64.86	80.11	79.70	68.77
	Ours	67.26	72.28	72.64	84.03	84.87	74.08	83.86	85.91	78.11
	U-HVED	17.58	20.39	32.17	67.75	70.11	28.94	69.60	70.09	47.07
	D2-Net	9.37	11.78	14.09	68.14	67.58	20.22	66.31	66.80	40.53
	Ours	42.58	44.27	47.14	76.12	74.95	46.83	76.91	77.61	60.80

Table 5. Ablation results for rare occurrence of FLAIR in training.

adapt meta-learning to distill discriminative features from full modality to partial modalities in an unified framework which discards the impractical omnipresence of full modalities. This mapping is further co-supervised by an adversarial learning that guarantees the generation of superior modality-agnostic representations. We also propose an attention-based aggregation block to unify the representations from multiple encoders, an engineering design essential for our model. In the future we plan to validate our method on other imaging modalities (such as multiplexed digital pathology) for different downstream tasks.

References

- [1] Antreas Antoniou, Harrison Edwards, and Amos Storkey. How to train your maml. In *ICLR*, 2019. [3](#)
- [2] Reza Azad, Nika Khosravi, and Dorit Merhof. Smu-net: Style matching u-net for brain tumor segmentation with missing modalities. In *MDL*, 2022. [1, 2](#)
- [3] Spyridon Bakas, Hamed Akbari, Aristeidis Sotiras, Michel Bilello, Martin Rozycki, Justin S Kirby, John B Freymann, Keyvan Farahani, and Christos Davatzikos. Advancing the cancer genome atlas glioma mri collections with expert segmentation labels and radiomic features. *Scientific data*, 2017. [1](#)
- [4] Mahsa Baktashmotlagh, Mehrtash T Harandi, Brian C Lovell, and Mathieu Salzmann. Unsupervised domain adaptation by domain invariant projection. In *ICCV*, 2013. [3](#)
- [5] Stefan Bauer, Roland Wiest, Lutz-P Nolte, and Mauricio Reyes. A survey of mri-based medical image analysis for brain tumor studies. *Physics in Medicine & Biology*, 2013. [1](#)
- [6] Moinak Bhattacharya, Shubham Jain, and Prateek Prasanna. Radiotransformer: A cascaded global-focal transformer for visual attention-guided disease classification. In *ECCV*, 2022. [2](#)
- [7] Agisilaos Chartsias, Thomas Joyce, Mario Valerio Giuffrida, and Sotirios A Tsaftaris. Multimodal MR synthesis via modality-invariant latent representation. *TMI*, 2017. [2, 3](#)
- [8] Cheng Chen, Qi Dou, Yueming Jin, Hao Chen, Jing Qin, and Pheng-Ann Heng. Robust multimodal brain tumor segmentation via feature disentanglement and gated fusion. In *MICCAI*, 2019. [2](#)
- [9] Jiayi Chen and Aidong Zhang. Hetmaml: Task-heterogeneous model-agnostic meta-learning for few-shot learning across modalities. In *CIKM*, 2021. [3](#)
- [10] Shengcong Chen, Changxing Ding, and Minfeng Liu. Dual-force convolutional neural networks for accurate brain tumor segmentation. *Pattern Recognition*, 2019. [1, 2](#)
- [11] Jae Won Cho, Dong-Jin Kim, Jinsoo Choi, Yunjae Jung, and In So Kweon. Dealing with missing modalities in the visual question answer-difference prediction task through knowledge distillation. In *CVPR*, 2021. [2](#)
- [12] Özgün Çiçek, Ahmed Abdulkadir, Soeren S Lienkamp, Thomas Brox, and Olaf Ronneberger. 3d u-net: learning dense volumetric segmentation from sparse annotation. In *MICCAI*, 2016. [8, 11, 12](#)
- [13] Yuhang Ding, Xin Yu, and Yi Yang. Rfnet: Region-aware fusion network for incomplete multi-modal brain tumor segmentation. In *ICCV*, 2021. [2, 3, 6, 7, 8, 11, 12, 13](#)
- [14] Reuben Dorent, Samuel Joutard, Marc Modat, Sébastien Ourselin, and Tom Vercauteren. Hetero-modal variational encoder-decoder for joint modality completion and segmentation. In *MICCAI*, 2019. [2, 3, 6, 7, 8, 11, 12, 13](#)
- [15] Changde Du, Changying Du, Hao Wang, Jinpeng Li, Wei-Long Zheng, Bao-Liang Lu, and Huiguang He. Semi-supervised deep generative modelling of incomplete multi-modality emotional data. In *ACM Multimedia*, 2018. [2](#)
- [16] Chelsea Finn, Pieter Abbeel, and Sergey Levine. Model-agnostic meta-learning for fast adaptation of deep networks. In *ICML*, 2017. [3](#)
- [17] Yaroslav Ganin and Victor Lempitsky. Unsupervised domain adaptation by backpropagation. In *ICML*, 2015. [3](#)
- [18] Martin J Graves and Donald G Mitchell. Body mri artifacts in clinical practice: a physicist’s and radiologist’s perspective. *Journal of Magnetic Resonance Imaging*, 2013. [1](#)
- [19] Arthur Gretton, Alex Smola, Jiaoyuan Huang, Marcel Schmitzfull, Karsten Borgwardt, and Bernhard Schölkopf. Covariate shift by kernel mean matching. *Dataset shift in machine learning*, 2009. [3](#)
- [20] Mohammad Hamghalam, Alejandro F Frangi, Baiying Lei, and Amber L Simpson. Modality completion via gaussian process prior variational autoencoders for multi-modal glioma segmentation. In *MICCAI*, 2021. [2](#)
- [21] Mohammad Havaei, Axel Davy, David Warde-Farley, Antoine Biard, Aaron Courville, Yoshua Bengio, Chris Pal, Pierre-Marc Jodoin, and Hugo Larochelle. Brain tumor segmentation with deep neural networks. *Media*, 2017. [1, 2](#)
- [22] Mohammad Havaei, Nicolas Guizard, Nicolas Chapados, and Yoshua Bengio. Hemis: Hetero-modal image segmentation. In *MICCAI*, 2016. [2, 3, 6, 7, 8, 11, 12, 13](#)
- [23] Minhao Hu, Matthias Maillard, Ya Zhang, Tommaso Ciceri, Giammarco La Barbera, Isabelle Bloch, and Pietro Gori. Knowledge distillation from multi-modal to mono-modal segmentation networks. In *MICCAI*, 2020. [1, 2](#)
- [24] Fabian Isensee, Paul F Jaeger, Simon AA Kohl, Jens Petersen, and Klaus H Maier-Hein. nnu-net: a self-configuring method for deep learning-based biomedical image segmentation. *Nature methods*, 2021. [8, 11, 12](#)

[25] Mobarakol Islam, Navodini Wijethilake, and Hongliang Ren. Glioblastoma multiforme prognosis: Mri missing modality generation, segmentation and radiogenomic survival prediction. *Computerized Medical Imaging and Graphics*, 2021. 1, 2

[26] Aishik Konwer, Joseph Bae, Gagandeep Singh, Rishabh Gattu, Syed Ali, Jeremy Green, Tej Phatak, and Prateek Prasanna. Attention-based multi-scale gated recurrent encoder with novel correlation loss for covid-19 progression prediction. In *MICCAI*, 2021. 2

[27] Aishik Konwer, Xuan Xu, Joseph Bae, Chao Chen, and Prateek Prasanna. Temporal context matters: Enhancing single image prediction with disease progression representations. In *CVPR*, 2022. 3

[28] Gueorgi Kossinets. Effects of missing data in social networks. *Social networks*, 2006. 2

[29] Kenneth Lau, Jonas Adler, and Jens Sjölund. A unified representation network for segmentation with missing modalities. *arXiv preprint arXiv:1908.06683*, 2019. 2

[30] Da Li, Yongxin Yang, Yi-Zhe Song, and Timothy Hospedales. Learning to generalize: Meta-learning for domain generalization. In *AAAI*, 2018. 3

[31] Han Liu, Yubo Fan, Hao Li, Jiacheng Wang, Dewei Hu, Can Cui, Ho Hin Lee, Huahong Zhang, and Ipek Oguz. Mod-drop++: A dynamic filter network with intra-subject co-training for multiple sclerosis lesion segmentation with missing modalities. In *MICCAI*, 2022. 2

[32] Mengmeng Ma, Jian Ren, Long Zhao, Sergey Tulyakov, Cathy Wu, and Xi Peng. Smil: Multimodal learning with severely missing modality. In *AAAI*, 2021. 3

[33] Yao Ma, Shilin Zhao, Weixiao Wang, Yaoman Li, and Irwin King. Multimodality in meta-learning: A comprehensive survey. *Knowledge-Based Systems*, 2022. 3

[34] Bjoern H Menze, Andras Jakab, Stefan Bauer, Jayashree Kalpathy-Cramer, Keyvan Farahani, Justin Kirby, Yuliya Burren, Nicole Porz, Johannes Slotboom, Roland Wiest, et al. The multimodal brain tumor image segmentation benchmark (brats). *TMI*, 2014. 6, 11

[35] Fausto Milletari, Nassir Navab, and Seyed-Ahmad Ahmadi. V-net: Fully convolutional neural networks for volumetric medical image segmentation. In *3DV*, 2016. 6

[36] Andriy Myronenko. 3d mri brain tumor segmentation using autoencoder regularization. In *MICCAI Brainlesion Workshop*, 2018. 1, 2

[37] Alex Nichol, Joshua Achiam, and John Schulman. On first-order meta-learning algorithms. *arXiv preprint arXiv:1803.02999*, 2018. 3

[38] Ozan Oktay, Jo Schlemper, Loic Folgoc, Matthew Lee, Matthias Heinrich, Kazunari Misawa, Kensaku Mori, Steven McDonagh, Nils Hammerla, Bernhard Kainz, Ben Glocker, and Daniel Rueckert. Attention u-net: Learning where to look for the pancreas. In *MIDL*, 2018. 8, 11, 12

[39] Adam Paszke, Sam Gross, Soumith Chintala, Gregory Chanan, Edward Yang, Zachary DeVito, Zeming Lin, Alban Desmaison, Luca Antiga, and Adam Lerer. Automatic differentiation in pytorch. In *NeurIPS Workshop*, 2017. 6

[40] Sylvestre-Alvise Rebuffi, Sebastien Ehrhardt, Kai Han, Andrea Vedaldi, and Andrew Zisserman. Semi-supervised learning with scarce annotations. In *CVPR Workshops*, 2020. 2

[41] Anmol Sharma and Ghassan Hamarneh. Missing mri pulse sequence synthesis using multi-modal generative adversarial network. *TMI*, 2019. 1, 2, 3

[42] Yan Shen and Mingchen Gao. Brain tumor segmentation on mri with missing modalities. In *IPMI*, 2019. 1, 2

[43] Jake Snell, Kevin Swersky, and Richard Zemel. Prototypical networks for few-shot learning. In *NeurIPS*, 2017. 3

[44] Baochen Sun and Kate Saenko. Deep coral: Correlation alignment for deep domain adaptation. In *ECCV*, 2016. 3

[45] Qianru Sun, Yaoyao Liu, Tat-Seng Chua, and Bernt Schiele. Meta-transfer learning for few-shot learning. In *CVPR*, 2019. 3

[46] Qilong Suo, Weida Zhong, Fenglong Ma, Ye Yuan, Jing Gao, and Aidong Zhang. Metric learning on healthcare data with incomplete modalities. In *IJCAI*, 2019. 2

[47] Yucheng Tang, Dong Yang, Wenqi Li, Holger R Roth, Bennett Landman, Daguang Xu, Vishwesh Nath, and Ali Hatamizadeh. Self-supervised pre-training of swin transformers for 3d medical image analysis. In *CVPR*, 2022. 1, 2, 6

[48] Saverio Vadacchino, Raghav Mehta, Nazanin Mohammadi Sepahvand, Brennan Nichyporuk, James J Clark, and Tal Arbel. Had-net: A hierarchical adversarial knowledge distillation network for improved enhanced tumour segmentation without post-contrast images. In *MIDL*, 2021. 1, 2

[49] Shanshan Wang, Cheng Li, Rongpin Wang, Zaiyi Liu, Meiyun Wang, Hongna Tan, Yaping Wu, Xinfeng Liu, Hui Sun, Rui Yang, et al. Annotation-efficient deep learning for automatic medical image segmentation. *Nature communications*, 2021. 2

[50] Wenxuan Wang, Chen Chen, Meng Ding, Hong Yu, Sen Zha, and Jiangyun Li. Transbts: Multimodal brain tumor segmentation using transformer. In *MICCAI*, 2021. 1, 2

[51] Yixin Wang, Yang Zhang, Yang Liu, Zihao Lin, Jiang Tian, Cheng Zhong, Zhongchao Shi, Jianping Fan, and Zhiqiang He. Acn: Adversarial co-training network for brain tumor segmentation with missing modalities. In *MICCAI*, 2021. 1, 2, 6, 7, 11, 13

[52] Qiushi Yang, Xiaoqing Guo, Zhen Chen, Peter YM Woo, and Yixuan Yuan. D2-net: Dual disentanglement network for brain tumor segmentation with missing modalities. *TMI*, 2022. 2, 6, 7, 13

[53] Biting Yu, Luping Zhou, Lei Wang, Jurgen Fripp, and Pierrick Bourgeat. 3d cgan based cross-modality mr image synthesis for brain tumor segmentation. In *ISBI*, 2018. 1, 2

[54] Ziqi Yu, Yuting Zhai, Xiaoyang Han, Tingying Peng, and Xiao-Yong Zhang. Mousegan: Gan-based multiple mri modalities synthesis and segmentation for mouse brain structures. In *MICCAI*, 2021. 1, 2, 3

[55] Yao Zhang, Nanjun He, Jiawei Yang, Yuexiang Li, Dong Wei, Yawen Huang, Yang Zhang, Zhiqiang He, and Yefeng Zheng. mmformer: Multimodal medical transformer for incomplete multimodal learning of brain tumor segmentation. In *MICCAI*, 2022. 2, 3, 6, 7, 13

[56] Zechen Zhao, Heran Yang, and Jian Sun. Modality-adaptive feature interaction for brain tumor segmentation with missing modalities. In *MICCAI*, 2022. 2, 3

[57] Chenhong Zhou, Changxing Ding, Xinchao Wang, Zhentai Lu, and Dacheng Tao. One-pass multi-task networks with cross-task guided attention for brain tumor segmentation. *TIP*, 2020. 1, 2

[58] Tongxue Zhou, Stéphane Canu, Pierre Vera, and Su Ruan. Conditional generator and multi-sourcecorrelation guided brain tumor segmentation with missing mr modalities. *arXiv preprint arXiv:2105.13013*, 2021. 1, 2

[59] Tongxue Zhou, Stéphane Canu, Pierre Vera, and Su Ruan. Latent correlation representation learning for brain tumor segmentation with missing mri modalities. *TIP*, 2021. 2, 3

Supplementary Material

In the supplementary material, we provide additional information to better understand the contributions and claims of our proposed work. Comprehensive results on BRATS2020 dataset are provided in Sec. 6. In Sec. 7 we provide the ablation results on additional tumor regions demonstrating the robustness of our approach to varying proportions of full modality data. In Sec. 8 further experiments are conducted to test the bias of our model to occurrence of a specific modality (FLAIR or T1c). The ablation results for various encoder-decoder backbones (3DUnet, nnUnet, AttentionUnet) are shown in Sec. 9. In Sec. 10 we discuss the architectural details for different fusion baselines. Qualitative segmentation maps are shown in Sec. 11. In Sec. 12 we report the standard deviation and statistical significance for DSC(%) results. Comparisons via HD95 are presented in Sec. 13.

6. Results on BRATS2020 dataset

In Tab. 6, we compare our approach with three state-of-the-art methods including HeMIS [22], U-HVED [14], and RFNet [13] for tumor segmentation on BRATS2020 dataset [34]. The average DSC of the three tumor areas are boosted by 1.78%, 2.84%, and 3.13%, respectively.

7. Additional ablation results on robustness to full modality

Ablation results on WT region have been provided in the main paper to demonstrate that our method performs well even with a limited number of full modality samples in training. Here we are providing additional results for TC and ET regions. We compare against ACN [51] and RFNet [13] by varying the full modality count from 100% to 40% (Fig. 7). In order to retain sufficient samples for each combination task in meta-training, we assume that at least 50% of the patients have partial modalities. Hence we

show our results only on 50% and 40% proportions of full modality data. Unlike other methods, ours shows only a minor decline in DSC (0.3%) for both TC and ET. These experimental results verify the hypothesis that the proposed method is robust to full modality setting.

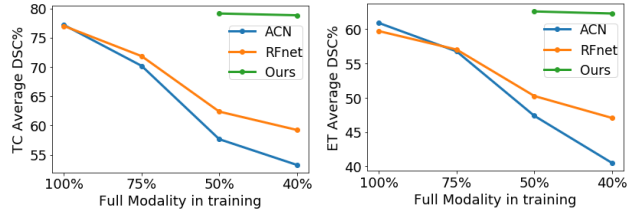


Figure 7. Ablation studies for varying % of full modality in training.

8. Additional ablation results on bias to presence of a specific modality

In the main paper we have provided ablation results on WT region by varying FLAIR proportion from 35% to 45%. Here we provide extensive results for the remaining two tumor regions (TC and ET). Fig. 8 suggests that on increasing FLAIR from 35% to 45%, our model’s DSC gain (for both TC and ET) is much less when compared to that of U-HVED or D2Net. This demonstrates that our approach is not sensitive to presence of any particular modality. Similar conclusions can also be drawn when experiments are carried out keeping T1c as the rarely occurring modality instead of FLAIR. The results are presented in Tab. 7 and Fig. 9.

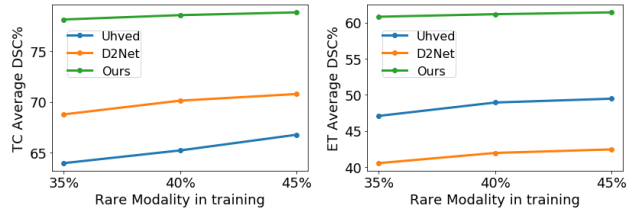


Figure 8. Ablation studies for varying % of FLAIR in training.

9. Ablation results on robustness to encoder-decoder backbones

We hypothesize that the proposed meta-learning and adversarial training strategies are independent of the backbones utilized in the framework. To confirm this, we evaluate our approach using different backbones including 3DUnet [12], nnUnet [24], and AttentionUnet [38]. The average DSC reported in Tab. 8 marginally varies between 1.25% and 2.6% across all encoder-decoder variants, indi-

M	FLAIR	○	○	○	●	○	○	●	○	●	●	●	●	○	●	Avg	
WT	HeMIS [22]	80.34	66.92	66.35	58.72	85.16	73.41	69.79	83.30	83.76	73.41	76.78	84.43	85.17	85.84	86.03	77.29
	U-HVED [14]	82.13	71.42	58.30	82.76	85.72	74.09	86.46	84.34	87.91	87.15	86.59	88.66	88.92	85.86	89.43	82.65
	RFNet [13]	86.30	76.34	77.72	87.05	88.02	81.07	89.72	88.02	89.64	89.51	90.44	90.62	90.55	88.50	91.01	86.96
	Ours	88.24	82.29	83.41	88.37	88.78	83.26	90.52	89.66	90.55	90.83	91.34	91.68	91.17	89.49	91.57	88.74
TC	HeMIS [22]	60.83	74.22	48.57	37.03	79.84	78.35	48.19	60.80	60.21	74.62	78.88	63.48	79.24	81.56	81.03	67.12
	U-HVED [14]	61.37	74.93	39.54	52.42	80.27	79.11	57.38	62.17	63.47	77.45	79.02	65.39	80.19	81.72	81.68	69.07
	RFNet [13]	70.94	82.45	65.58	69.88	85.82	83.88	72.76	72.90	73.45	85.71	85.97	74.74	86.11	85.55	86.24	78.79
	Ours	73.56	86.37	74.69	72.33	87.71	87.52	75.94	74.50	76.24	87.79	87.82	76.93	87.31	87.98	87.75	81.63
ET	HeMIS [22]	32.78	64.95	20.41	14.63	71.12	71.40	19.04	29.76	30.66	69.52	71.39	32.13	71.98	72.37	72.44	49.64
	U-HVED [14]	31.86	68.43	18.21	25.85	70.48	70.79	27.94	32.37	33.64	71.24	72.16	34.48	71.72	71.92	71.87	51.53
	RFNet [13]	48.03	74.84	36.58	38.45	76.66	76.52	43.12	51.40	51.02	76.38	77.10	49.82	77.07	78.10	77.02	62.14
	Ours	52.77	80.06	42.28	44.87	78.92	79.85	46.73	54.67	54.29	78.81	77.31	50.69	79.24	79.43	79.12	65.27

Table 6. Comparison with state-of-the-art for the different combinations of available modalities on BRATS2020. Dice scores (DSC %) are computed for three nested tumor subregions - Whole tumor (WT), Tumor core (TC), Enhancing tumor (ET). Modalities present are denoted by ●, the missing ones by ○.

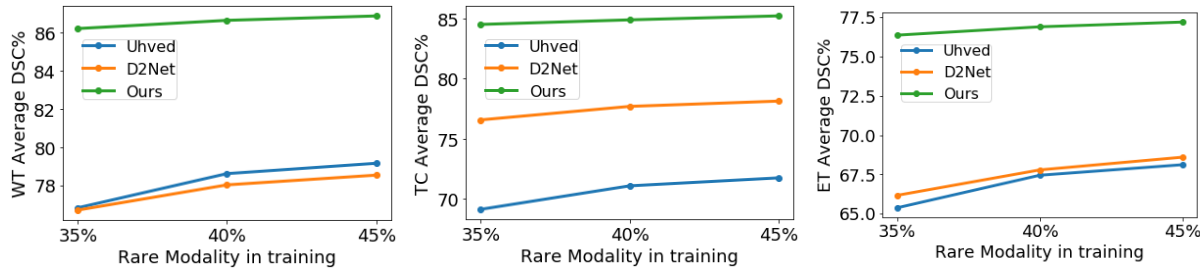


Figure 9. Ablation studies for varying % of T1c in training.

M	FLAIR	○	○	○	●	●	●	○	●	●	●	●	○	●	Avg
WT	U-HVED	54.38	77.63	63.70	82.28	84.06	84.96	81.19	86.37	76.82					
	D2-Net	39.14	81.57	62.77	86.32	85.98	87.85	82.40	87.53	76.70					
	Ours	78.46	85.71	78.83	89.22	89.64	90.08	87.19	90.57	86.21					
TC	U-HVED	61.16	70.87	62.21	70.65	72.24	70.59	74.52	70.87	69.13					
	D2-Net	61.73	78.46	75.31	80.69	78.17	79.85	78.77	79.58	76.57					
	Ours	83.62	84.79	83.56	84.18	84.35	83.88	85.80	85.94	84.51					
ET	U-HVED	57.23	65.39	62.08	65.76	68.15	67.81	67.26	69.42	65.38					
	D2-Net	65.13	66.37	67.84	65.41	65.06	65.33	67.98	66.27	66.17					
	Ours	77.02	75.98	76.43	76.25	75.11	76.67	75.89	77.54	76.36					

Table 7. Ablation results for rare occurrence (35%) of T1c in training. ● for T1c in all combinations denote that T1c is always present in inference despite being rare on training.

cating that our method is robust to such architectural designs.

Methods	Average DSC%		
	WT	TC	ET
3DUnet [12]	85.70	77.87	59.93
AttentionUnet [38]	86.02	78.05	60.46
nnUnet [24]	86.53	78.64	62.28
Ours	87.12	79.12	62.53

Table 8. Ablation on backbones

10. Architectural details of fusion baselines

The architectures of the three fusion baselines, (a) Sum, (b) Average, and (c) Att-Pool are illustrated in Fig. 10. For the first two approaches, feature maps from available modalities are summed or averaged along the channel dimension C to obtain the fused feature. In the third approach, available modality features are individually passed through a Global Average Pooling (GAP) layer. The GAP outputs are fed to a Fully Connected Network (FCN) followed by softmax activation function, producing the attention weights of each modality. Finally attention-weighted summation of the original modality features gives rise to the fused feature. However, our proposed aggregation block explicitly exploits the interaction between channels from the available modalities. Such inter-modality relations improve the quality of the fused embedding.

11. Qualitative comparison

In Fig. 11 we visualize the segmentation masks predicted by U-HVED, RFNet, and our method from four combinations of modalities in the inference phase. Unlike other methods, our segmentations do not degrade sharply as addi-

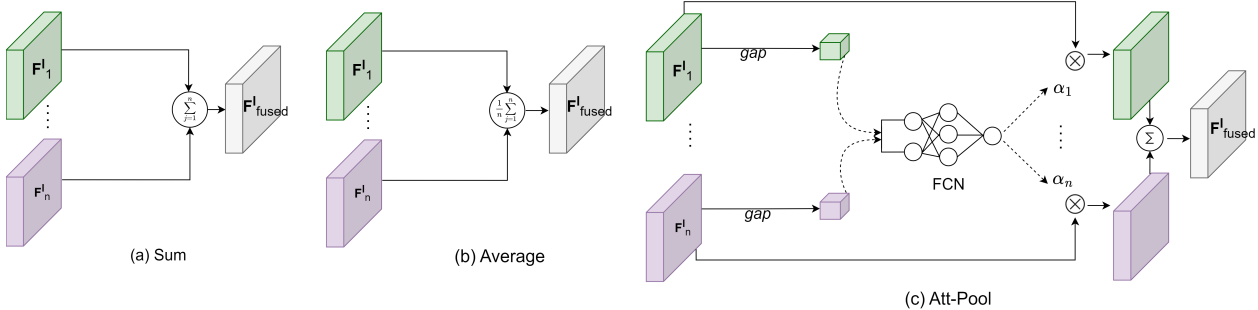


Figure 10. Fusion baselines

tional modalities are dropped during inference. Even with single T2 or T1+T2 modalities, our model achieves higher DSC scores.

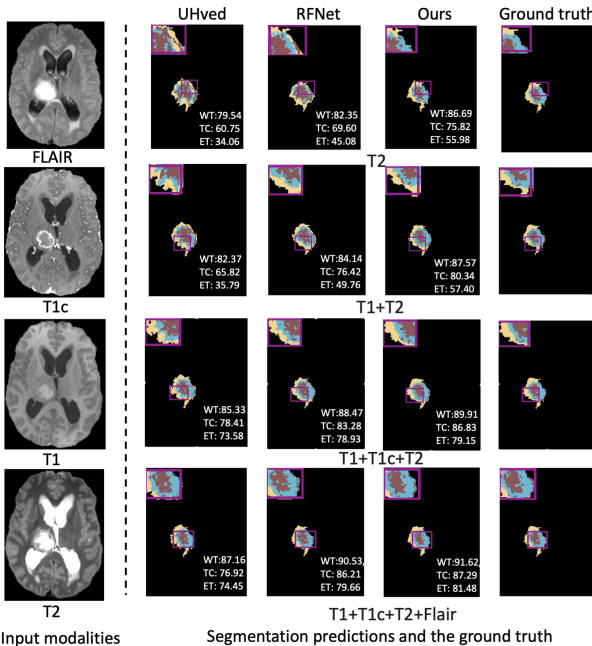


Figure 11. Qualitative comparisons with SOTA. Column 1: four MRI modalities. Column 2-4: segmentation maps predicted by three methods for different combinations of modalities. Column 5: Ground truth.

12. Measure of variation and statistical significance

We report DSC standard deviations (std) with p-values in Tab. 9. Our results are statistically significantly better ($p < 0.05$) than [14, 22, 52]. Other methods [13, 51, 55] require full modality input for all samples; ours doesn't.

13. Additional evaluation metric

We computed Hausdorff Distance (HD95) as another evaluation metric. It can be observed from Tab. 10 that

Methods	Average DSC (%), P-value (10^{-2})		
	Complete	Core	Enhancing
HeMIS [22]	76.23 \pm 9.66, 0.05*	58.57 \pm 15.50, 0.01*	45.11 \pm 24.97, 3.23*
U-HVED [14]	79.55 \pm 11.14, 2.10*	64.55 \pm 10.72, 0.02*	48.44 \pm 22.98, 6.41
D2-Net [52]	77.04 \pm 19.95, 6.64	67.65 \pm 16.55, 2.02*	45.22 \pm 26.52, 4.07*
ACN [51]	85.25 \pm 3.38, 20.43	77.16 \pm 7.56, 47.26	60.85 \pm 17.12, 78.65
RFNet [13]	85.75 \pm 6.03, 48.41	76.99 \pm 7.00, 41.76	59.67 \pm 16.85, 64.25
mmFormer [55]	86.25 \pm 5.16, 62.41	74.89 \pm 6.46, 10.09	55.88 \pm 13.86, 24.25
Ours	87.12\pm4.43	79.12\pm7.18	62.53\pm16.53

Table 9. Standard deviation and statistical significance for DSC(%) on BRATS2018 our method outperforms SOTA in 2/3 regions (WT, TC) and emerges second-best for ET on BRATS2018.

Methods	Average HD95(↓), P-value(10^{-2})		
	Complete	Core	Enhancing
HeMIS [22]	14.85 \pm 7.32, 0.08*	15.58 \pm 8.44, 0.16*	19.65 \pm 12.37, 0.25*
U-HVED [14]	13.64 \pm 6.27, 0.12*	14.91 \pm 7.19, 0.09*	18.43 \pm 11.68, 0.42*
D2-Net [52]	10.82 \pm 6.70, 7.75	11.76 \pm 7.35, 5.12	14.79 \pm 8.79, 1.75*
ACN [51]	8.15 \pm 2.03, 39.05	9.37 \pm 2.81, 8.39	8.62\pm2.43, 86.77
RFNet [13]	7.89 \pm 1.72, 58.64	8.43 \pm 2.52, 42.09	12.56 \pm 3.68, 0.36*
mmFormer [55]	7.67 \pm 2.14, 84.97	8.06 \pm 2.41, 69.59	10.54 \pm 3.13, 11.41
Ours	7.53\pm1.86	7.73\pm2.16	8.78 \pm 2.77

Table 10. Comparison with HD95 distance metric

14. Evaluation of enhanced representations

We pass the fused representations \mathbf{F}_{fused}^l of 50 test patients (scenarios of Partial: T1c, T2 present and Full: All present) from the baseline and our method into a classifier trained to predict the probabilities (prob) of a modality's presence. Our average probabilities are comparable across partial and full modality scenarios (Fig. 12), depicting the desired enhancement of \mathbf{F}_{fused}^l . E.g.: Red box depicts how our prob for predicting T1 are considerably higher than the baseline even in T1-missing scenario.

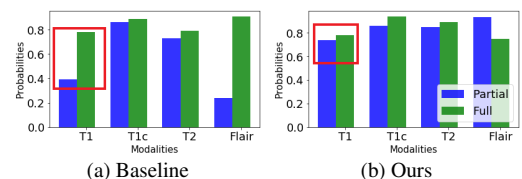


Figure 12. Comparison of baseline and enhanced representations

15. Additional implementation details

Learning rate (LR: 5e-5), λ_1 : 0.8, λ_2 : 0.2, and scale of discriminator (Sc: 0.5) were selected based on the model performance. Results with different sets of parameters are shown in Tab. 11.

LR	WT DSC(%)	λ_1, λ_2	Avg DSC % (WT, TC, ET)	Sc	WT DSC(%)
5e-3	86.79	0.9, 0.1	86.89, 78.94, 62.37	0.25	86.44
5e-4	86.95	0.8, 0.2	87.12, 79.12, 62.53	0.5	87.12
5e-5	87.12	0.7, 0.3	86.97, 78.83, 62.19	0.6	87.03

Table 11. Selection of experimental parameters